INTERFERENCE BETWEEN COHERENCES ESTABLISHED AMONG THE $5D_{5/2}$ – $5P_{3/2}$ AND $5P_{3/2}$ – $5S_{1/2}$ ENERGY LEVELS WITHIN ATOMIC RUBIDIUM

BY

THOMAS REBOLI

THESIS

Submitted in partial fulfillment of the requirements
for the degree of Master of Science in Electrical and Computer Engineering
in the Graduate College of the
University of Illinois Urbana-Champaign, 2022

Urbana, Illinois

Adviser:

Professor J. Gary Eden

ABSTRACT

Coupling was observed between atomic coherences formed at 386.2 THz and 384.1 THz, corresponding respectively to the $5D_{5/2} - 5P_{3/2}$ and $5P_{3/2} - 5S_{1/2}$ energy differences in atomic Rb. These coherences were excited using ultrafast laser pulses, and their temporal dynamics observed through quantum beat spectroscopy. The coupling of these oscillators was observed as an interference window occurring in the spectral response of the pair's beat frequency. The spectral profile of these pairs was also observed to change with varying phase matching conditions. The profile was fit to a generalized Fano resonance to recover phase, which corresponds to degree of coupling between the states. The profile was also found to change with experimental parameters, giving control over the coupling parameters.

To the eternal slog of science.

ACKNOWLEDGMENTS

I would like to first thank my family for their tireless support and encouragement in my pursuit of higher education. To my parents, thank you for planting the seeds that eventually grew into a love of science. You never stopped pushing me to try new things, and always encouraged me to do my best. You gave me a space where I could learn from my own mistakes without fear of judgment. To Bernice Wang, my girlfriend of nine years, I can confidently say that I would not have made it nearly this far without your constant love and support. Even when you are 2000 miles away, it feels like you are right next to me, pushing me forward. Sorry there have been so many delays in my proposal.

In my short time as a graduate student, I have had the pleasure of working with some of the most inspirational and hardworking people I have ever met. Gary, I cannot imagine having a better advisor. Your enthusiastic meetings are inspiring, and I leave each one with the urge to run the lab to start working immediately. Your endless optimism has pushed me to accomplish things that I would have given up on far sooner. Kavita, I still remember our undergraduate lab classes like they were yesterday. You are always ready with a smile and a bad joke to start my mornings, and are a never-ending source of good advice, both academic and personal. I would also like to thank all the members of LOPE for being incredibly welcoming. From our very first group meeting I felt included, and now the office feels like a home away from home.

I would also like to thank all those who worked on this quantum beating experiment long before me, both those I have met and those who have graduated. Sehyun, thank you for being a guiding hand during my first semester of graduate school. Though we were unable to work together for long, your expertise helped me gain the confidence I needed to work on a project alone.

Finally, I would be remiss to ignore my brief time in industry. To Rick

Casler and Dave Fromm, I would like to extend my deepest thanks for the interest you both took in me as a young college student. You both helped to instill the dedication and work ethic required to succeed in graduate school, and encouraged me to push my education even further.

TABLE OF CONTENTS

CHAPTER 1

INTRODUCTION

Manipulation of quantum coherences within atoms has seen an increase in popularity over the past several years. While their application as qubits for quantum computing is the primary driving factor [1], exploration of these coherences and possible coupling behavior between them is of interest to the world of physics in general. Careful fabrication of bulk material and metasurfaces allows for a high level of control over resonances and coupling, producing custom optical properties [2]. However, while these effects have been studied in manufactured materials, little research has been performed on coupling between atomic coherences.

1.1 Quantum Beat Spectroscopy

A possible method of investigating coupling between atomic oscillators is through quantum beat spectroscopy (QBS). This time resolved, Doppler free, high resolution spectroscopic method is capable of measuring the energy separations between closely spaced energy levels with sub-megahertz precision. More importantly, it accomplishes this by establishing a coherent superposition of excited states and observing the subsequent interference produced during radiative decay of the wave packet. The initial theory for QBS was laid out by Corney in 1964 [3], with experimental results measuring Zeeman splitting of the $^3P_1$ level of atomic Hg published later that same year [4]. In the decades following, QBS has found applications in both atomic and molecular spectroscopy, observing features such as Zeeman splitting, high principal quantum number states, and molecular rovibrational states [5–8].

To investigate the mechanics behind QBS, a simple four-level atomic system can be used. An example of this kind of system is shown in Figure 1.1. When excited by a spectrally broad pulsed laser source, both of the upper

energy levels $|2\rangle$ and $|3\rangle$ have some probability of being excited. This forms a non-stationary superposition of both energy level's wave functions:

$$|\Psi(t)\rangle = c_2 e^{-i\omega_2 t}|2\rangle + c_3 e^{-i\omega_3 t}|3\rangle \tag{1.1}$$

These wave functions continue to evolve in time before eventually decaying to the intermediate state $|4\rangle$ via emission of a photon. The overall emission intensity can be represented as:

$$I = |\langle 4|\mu|\Psi(t)\rangle|^2 \tag{1.2}$$

This intensity term can be expanded using the $|\Psi(t)\rangle$ defined in Equation 1:

$$I = c_2^2|\langle 4|\mu|2\rangle|^2 + c_3^2|\langle 4|\mu|3\rangle|^2 + c_2 c_3 \langle 4|\mu|2\rangle\langle 4|\mu|3\rangle(e^{-i(\omega_2-\omega_3)t} + e^{i(\omega_2-\omega_3)t}) \tag{1.3}$$

$$I \propto \cos(\Delta\omega t) \qquad \Delta\omega = \omega_2 - \omega_3 \tag{1.4}$$

The first two terms in Equation 1.3 are constant background emission caused by the natural decay of the wave packet through one of the two possible decay channels. The third term acts as a modulation effect on the emission intensity. As can be seen in Equation 1.4, the frequency of this modulation is directly related to the difference in frequency, and thus energy, of the two excited states. This math extends to any number of excited states as well, with the resulting decay emission from a wave packet of n states being modulated by $\binom{n}{2}$ frequencies. Additionally, modulation will also occur on all subsequent decays to the ground state. For example, if there is a radiative process from $|4\rangle$ to $|1\rangle$, that emission will also have the same modulation frequency applied to it. This is due to the imprinting of the wave packet information onto state $|4\rangle$ during the initial decay process [6, 9]:

$$|4\rangle = |4\rangle\langle 4|\mu|\Psi\rangle \tag{1.5}$$

$$|4\rangle = (c_2\langle 4|\mu|2\rangle e^{-i\omega_2 t} + c_3\langle 4|\mu|3\rangle e^{-i\omega_3 t})|4\rangle \tag{1.6}$$

From the previous equations, it is straightforward to understand some of QBS's most important features. First, as mentioned previously, measurements avoid Doppler broadening. This is a spectral broadening effect that

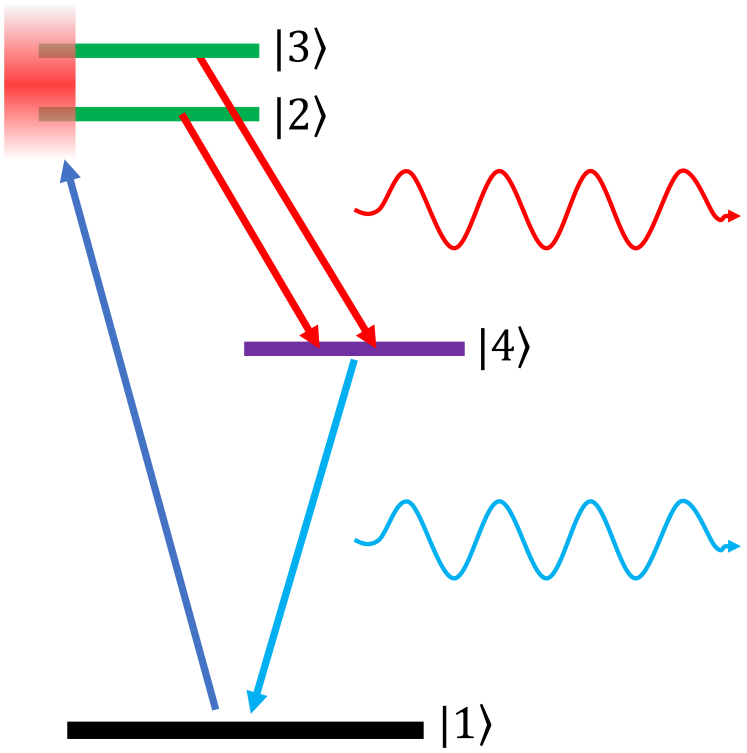

Figure 1.1: Excitation process that results in observable quantum beats. A broadband source, represented by the red gradient and wide enough to encompass multiple energy levels, generates a superposition of states. When these states decay, the emitted intensity will be modulated by the energy separation of the states, represented by the red wavy line. Subsequent decay emissions will also be modulated, as represented by the blue wavy line.

occurs when the motion of the atom or molecule in question red- or blue-shifts the energy levels. This produces a continuous spectrum of possible absorption or emission wavelengths that depend on temperature of the sample. For a hot atomic vapor, this broadening can be on the order of hundreds of megahertz [10]. QBS circumvents this issue by decoupling the measurement from the kinetics of the sample. The measured modulation frequency is determined by the energy differences between states within the sample, which are invariant under temperature change. This feature made it appealing to those studying the small energy spacing listed earlier. The second important feature, and one more applicable to the topic being studied in this thesis, is the fact that the intensity measurement is in the time domain. While this allows measurements of low frequency modulation signals to be easily sampled, it also means that, should enough oscillations be captured, the temporal evo-

lution of the wave packet can be evaluated through the changing responses present in the modulation. However, this also requires either a very long emission lifetime, or very large energy separation, to perform. The latter of these will be considered in this thesis, as the states being excited have an energy separation in the terahertz.

While much effort has been dedicated toward closely separated energy levels, investigations of gigahertz and terahertz separations are technically possible. Several challenges do exist when transitioning to this higher energy region, as there is a trade-off between ease of detection and energy separation. Narrow spacings, like the aforementioned Zeeman splittings or high principal quantum number states, are easy to detect, as most transient digitizers allow sample rates well over 1 GHz. They are also easy to excite with a naturally broad pulsed laser, without having to resort to ultra-fast systems. Larger energy gaps are not completely inaccessible, as ultrafast laser systems can produce upwards of 10 THz of spectral bandwidth when transform limited. The issue instead lies in detection, as the emission will be modulated at a frequency beyond the resolvability of any detector. To solve this issue, a pump-probe method can be employed. This lifts the requirement to measure the intensity modulation in real time, instead measuring the intensity point by point. The wave packet is first excited with an initial pulse, then sampled by a temporally delayed probe pulse. Varying the delay between the pump and probe pulses allows the full temporal signal to be reconstructed piecewise over many excitation-sample cycles [8, 11, 12].

In this thesis, a specific two photon transition in atomic Rb will be primarily considered. This transition serves to coherently excite both the $7S_{1/2}$ and $5D_{5/2}$ states, which have an energy separation of about 18 THz. The atomic structure with applicable energy levels is shown in Figure 1.2. Although the excitation of these two states is prioritized in the wave packet, other parasitically excited states will occur. Due to the large energy separation between these two states, the aforementioned pump-probe method must be employed. While the probe's excitation process involves a two photon transition, the corresponding probe's sampling process is done through parametric four wave mixing. This process produces two modulated emission frequencies, an idler emitting from the wave packet to the $6P_{3/2}$ state and a signal emitting from the $6P_{3/2}$ to the $5S_{1/2}$ state. These emissions occur at 60 THz and 420 nm respectively. While both could theoretically be used

to measure the quantum beat signature, the 420 nm signal is far easier to detect, thus the 60 THz idler will be ignored [12, 13]. The choice of time delay in the pump-probe setup is small enough that transient excitation behaviors can be observed in the signal with sub-picosecond precision. Found within these responses is evidence of coupled oscillators via the appearance of an interference window. Additionally, there is evidence that the coupling strengths between these oscillators is controllable through adjustments to the phase matching conditions of the excitation process [14]. Chapter 2 will outline the experimental setup used, followed by presentation and summary of results in Chapter 3.

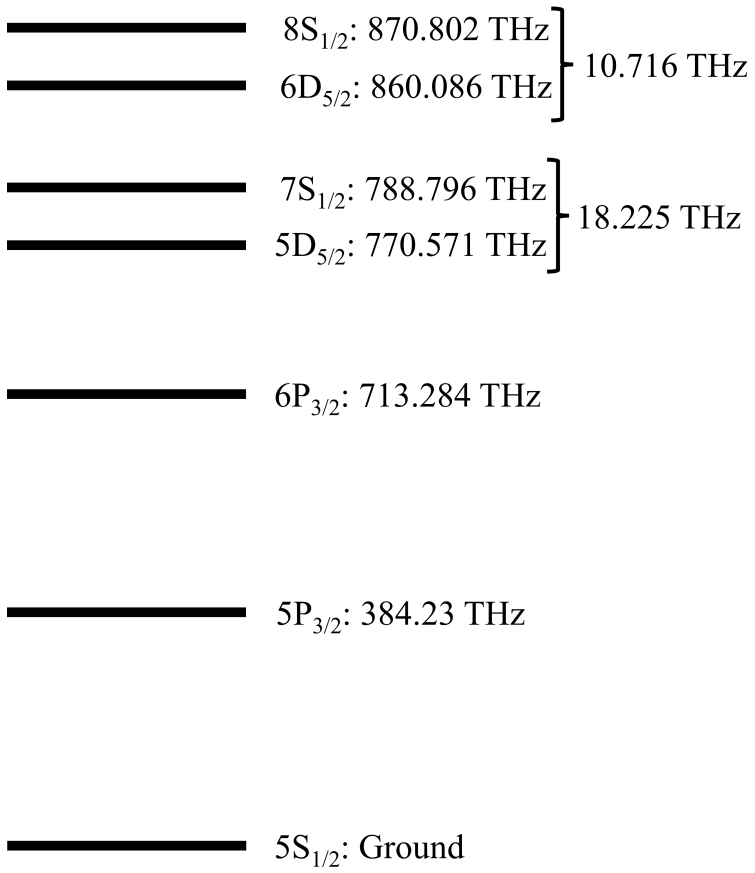

Figure 1.2: Abbreviated energy structure of Rb. Only states referenced in this thesis are listed. Coherences are generated among the $7S_{1/2}$ and $5D_{5/2}$ states due to their ease of access through two photon absorption. Observation of quantum beats is performed on the emission from the $6P_{3/2}$ state. Energy values retrieved from NIST energy level database and converted to terahertz for convenience [15].

1.2 Fano Resonances

Fano resonances are a type of asymmetric line-shape that occurs when a bound state interferes with a continuum of states. Although now seen in a variety of spectra, this effect was originally observed in noble gas spectra, namely He. Above the ionization level of He, there exists the doubly excited 2S2P state. Because this resonance lies within the ionization continuum of He, the two excitation pathways compete and interfere, producing a Fano line-shape. This process was first described mathematically by Fano in 1961 [16], later being generalized by Durand in 2001 [17]. This generalization improves on Fano's theory by including the linewidth of the continuum as well as the resonance. This forces the profile to tend toward zero at zero energy, which is more physical than Fano's, which tends toward one. The necessary equations for performing Fano profile fittings are given below:

$$I(E) = R(E)C(E)$$

$$R(E) = \frac{(\epsilon + q)^2}{1 + \epsilon_R^2} \qquad C(E) = \frac{1}{1 + \epsilon_C^2}$$

$$\epsilon_i = \frac{2}{\Gamma_i(E - E_i)} \qquad q = \cot(\theta)$$

These profiles are determined by five main parameters:

- $\Gamma_R \backslash \Gamma_C$: Linewidth of the resonance and continuum, respectively. Smaller values of the former produce more drastic interference windows, while larger values of the latter produce broader features.
- $E_R \backslash E_C$: Energy location of the resonance and continuum, respectively. Although usually similar, a larger offset between the two produces a larger degree of asymmetry.
- $q \backslash \theta$: Fano parameter and phase of the continuum, respectively [2].

In a classical sense, this effect can be considered as a pair of weakly coupled oscillators. A driven, dampened oscillator weakly coupled to a second will have a broad frequency response, acting as a continuum. The undampened oscillator will then act as a bound state that competes with the dampened oscillator. As the driving frequency transitions through the resonance frequency of one of the oscillators, there is an abrupt change in its phase. Since

this only happens to one of the oscillators, the pair will end up out of phase with each other. This in turn produces a zero point in the frequency response. The sudden phase shift just after the resonance frequency is what produces the asymmetric line-shape, examples of which are shown in Figure 1.3 [18].

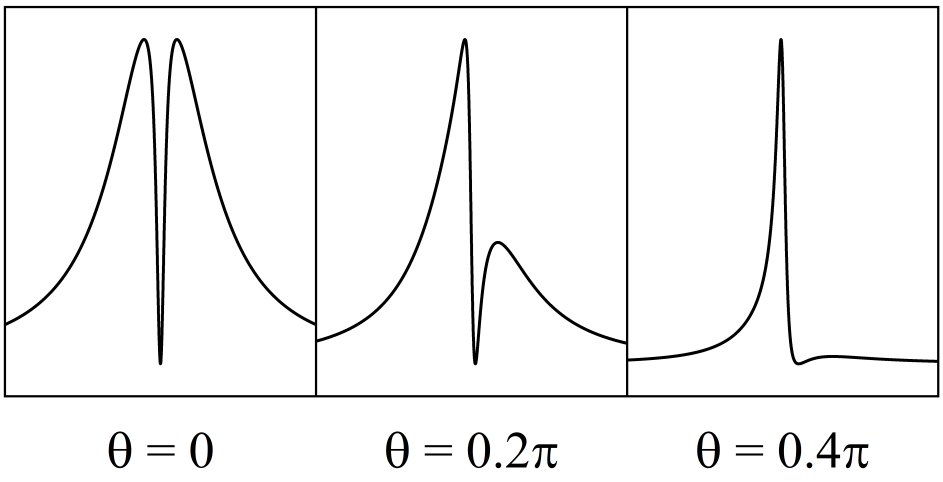

Figure 1.3: Examples of various Fano resonances. Increasing q value represents higher probabilities of exciting the resonance over the continuum. At lower q values, the spectrum is dominated by the broad continuum with a centered interference window. As coupling increases, and the resonance is excited more than the continuum, the profile becomes narrower, resulting in a pure Lorentzian at $q = \infty/\theta = \frac{\pi}{2}$.

CHAPTER 2

EXPERIMENTAL SETUP

The experimental setup consists of four main parts: a laser source, a Mach-Zender device, a sample, and a detector. A simplified diagram of the entire setup is presented in Figure 2.1. All parts work together to create a system capable of probing low principal quantum number states of atomic Rb via the pump-probe sampling method outlined in Chapter 1. The laser source is a Coherent Legend Elite HE+ ultrafast amplifier, henceforth referred to simply as the source. It is seeded with an 80 MHz femtosecond pulse train generated from a Coherent Vitara-S Ti:Sapphire mode locked laser oscillator. Individual pulses are picked off from this train and amplified through chirped pulse amplification to a maximum pulse energy of 3 mJ, controllable through the use of a computer controlled polarizer placed immediately after the regen cavity. The compressor grating within the source is also mounted on a motorized stage, allowing manual adjustment of compressor settings. This allows the pulse length to be controlled, as well as small amounts of chirp added to the pulse, which can help the formation of coherent wave packets [19]. The output of the source has a repetition rate of 1 kHz, with a typical pulse length when fully compressed of 50 fs and a typical spectral width of 20 nm at full width at half maximum. Each pulse is centered at 768 nm, facilitating the previously mentioned two photon transition to the $7S_{1/2}$ and $5D_{5/2}$ states. Because this transition requires two photons, the total bandwidth for the excitation processes is doubled. This allows for a total range of excitation from 769 THz to 791 THz, and since our targeted energy levels lie at 788.8 THz and 770.6 THz respectively, excitation of a wave packet is possible.

The amplified femtosecond pulses travel first through a set of telescoping optics to reduce the beam size to better match the size of the sample. Each pulse is then split with a 50% beamsplitter into a Mach-Zender device, forming the two pulses required in the pump-probe setup. One arm of

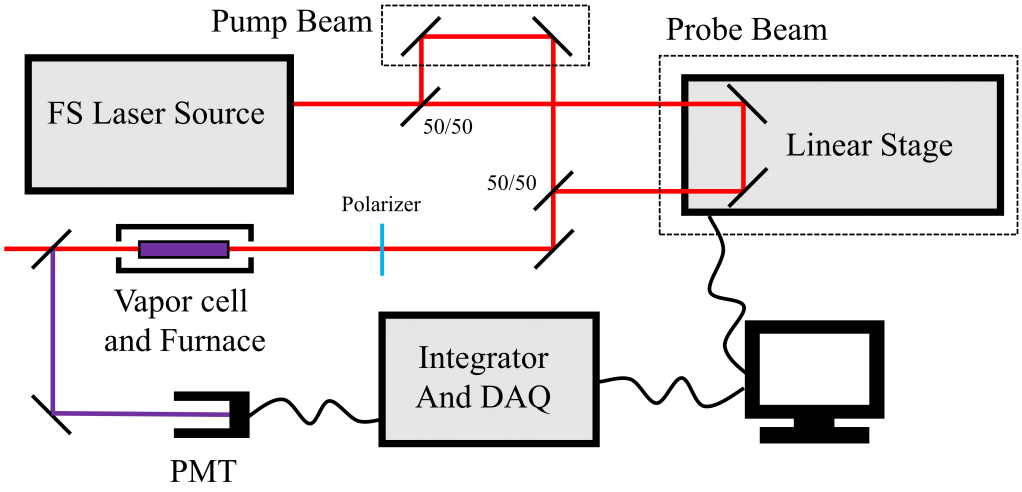

Figure 2.1: Simplified experimental setup for observing quantum beats. A femtosecond laser pulse is split into two identical pulses, with a time delay induced between them using a linear stage. Pulse pairs are used to probe a thermalized vapor held in a furnace. Emitted light is filtered and fed into a photomultiplier tube (PMT), which is integrated and sampled via a computer controlled data acquisition unit (DAQ).

this device is kept stationary, producing a pulse that will have a constant time. This pulse will be referred to as the pump pulse, and will be responsible for exciting the wave packet at the same point in time during every scan. The second arm in the device has its mirrors mounted on a Physik Instrumente M-521.DDB translational stage. This stage is capable of making individual steps of 500 nm with an accuracy of 100 nm. It has a maximum range of 204 mm, but due to stage positioning and time constraints, only 100 mm was used to produce a total temporal scan range of 600 ps. By changing the position of the mirrors with the stage, a variable time delay can be introduced between the pump and probe pulses. This is what allows the pump-probe setup to perform a temporal measurement. The chosen step size of 500 nm translates to a temporal resolution of 3.3 fs, a sampling rate of about 300 THz and a maximum detectable frequency of 150 THz due to the Nyquist theorem. This is more than enough to measure the targeted energy separation, and the excessive bandwidth allows for other responses to be visible and helps with temporal analysis of the wave packet. The separate arms are then recombined using a second 50% beamsplitter. The angle between the two pulses is also controllable using the mirrors and beamsplitter, which is necessary to adjust for phase matching conditions within the sample. A

polarizing beamsplitter is installed immediately before the furnace, which allows only polarization parallel to the optical table to pass into the furnace.

The sample consists of isotopically pure ^{85}Rb placed in an evacuated T-shaped Pyrex cell manufactured by Precision Glassblowing. The head of the cell is 25 mm long with a diameter of 12.5 mm. Each face is angled at 11 degrees to prevent reflections and Fabry-Pérot effects. This portion of the cell is where the pump and probe pulses will pass through the Rb to produce the quantum beating signal. The fill tube used to evacuate the cell and deposit the Rb is left attached to serve as a cold finger on the cell, accumulating condensed Rb and preventing it from depositing on the cell walls. The cell is placed in a ceramic heater with two controlled heating zones, one for the head and one for the stem. The temperature in the stem controls the number density of the vapor in the head, while the head is kept at a constant 25 K above the stem temperature, again to prevent condensation.

As mentioned previously, the quantum beat signal is carried on the 420 nm emission from the $6P_{3/2}$ state. This frequency is filtered off from the remaining pump and probe frequency with two UV coated mirrors and fed into a Hamamatsu H10721 photomultiplier tube. To protect from any residual light from the source or the room, a bandpass filter centered on the signal wavelength is also installed in front of the tube. The tube's output is fed to a Stanford Research Systems SR250 Gated Integrator, which is sampled by a National Instruments DAQ. The data acquisition is accomplished through an automated computer program, triggered off of the source's delay generator. Not included in the image is a MesaPhotonics FROGscan frequency resolved optical gating device, used to monitor pulse shape, spectral width, and other characteristics during measurements.

CHAPTER 3

RESULTS

3.1 Spectroscopic Results

Figure 3.1 presents a typical temporal scan taken using the setup detailed in Chapter 2. The upper plot is the raw output from the integrator as the linear stage was swept over 100 mm of travel. The small inset plot demonstrates the strength of the oscillations, as well as the long coherence lifetime of the wave packet, extending well beyond the length of the scan. The lower plot is the Fourier transform of the above temporal data. Several features within this plot are immediately evident, corresponding to different excited energy levels within the wave packet. These differences can be compared to the NIST values of Rb energy levels, previously shown in Figure 1.2, to confirm what states have been excited. The first and most prominent response is the one at 18.225 THz (Figure 3.1a), corresponding to the energy separation between the $7S_{1/2}$ and $5D_{5/2}$ states. When compared to published values, this difference is accurate to an error percentage of 0.01%, confirming that these are the states being excited. The small peak at 2.109 THz (Figure 3.1c) corresponds to the difference between two transitions, the $5D_{5/2} - 5P_{3/2}$ transition and the $5P_{3/2} - 5S_{1/2}$ transition (abbreviated as 5S-P-D). Comparing this to published values, the difference is accurate to 0.1%, also confirming the presence of these coherences. Since these are not accessible through the same two photon transition as the $7S_{1/2}$ and $5D_{5/2}$ states, a series of single photon transitions is instead believed to be responsible. Another response at 10.733 THz (Figure 3.1b) corresponds to $8S_{1/2}$ and $6D_{5/2}$ states. Again comparing to published values, this difference is accurate to 0.15%, also confirming these states as present in the wave packet. It is currently not fully understood how these states are being excited, as they lie well beyond what should be excitable with the available source wavelength. Current theory attributes

the phenomenon to the excitation of Rb-Rb dimers which later dissociate, leaving one excited in either the $8S_{1/2}$ or $6D_{5/2}$. Further discussion on this, as well as the higher harmonics (Figure 3.1d) and various difference frequencies that populate the response, can be found in Dr. William Goldshlag's dissertation [9].

3.2 Temporal Response and Analysis

Another scan is shown in Figure 3.2, prioritizing the generation of coherences among the 5S-P-D transitions. This was done by adjusting either the crossing angle or the number density of the vapor. Increasing the crossing angle produced a stronger response between these states, while increasing number density by increasing the furnace temperature suppressed the response. Pulse width and chirp also play a role, with longer, more negatively chirped pulses improving the response to a lesser degree. This plot highlights the benefit of performing a time domain measurement. Overall, the 5S-P-D coherence is very short lived, dying out within 150 ps. Under 5 ps, the coherence actually dominates the intended $7S_{1/2} - 5D_{5/2}$ coherence. To fully explore the time dependence of these coherences, a short time Fourier transform (STFT) was performed, shown in Figure 3.3. This allows the magnitude of each response, and by extension the composition of the wave packet, to be monitored as a function of time. Figure 3.4 uses the STFT to plot the evolution of the 5S-P-D coherence against the $7S_{1/2} - 5D_{5/2}$ coherence. The rapid decay previously observed is still apparent, with a lifetime of roughly 150 ps. What is also apparent is the synchronous increase in strength of the 18 THz response. This effect can also be seen qualitatively in Figure 3.2, and implies some degree of interaction between the two, wherein energy is being transferred from the 5S-P-D coherence into the $7S_{1/2} - 5D_{5/2}$. This process also appears to be unidirectional, with no energy flowing back into the 5S-P-D coherence at any time during the scan.

Figure 3.5 shows another plot from the STFT, tracking the 10.7 THz response of the $8S_{1/2}$-$6D_{5/2}$ coherence. This transition is an excellent example of the power of temporal wave packet analysis. The response is relatively weak for the first 400 ps of the scan, before abruptly and significantly increasing by a factor of 5. While more investigation into this effect is needed,

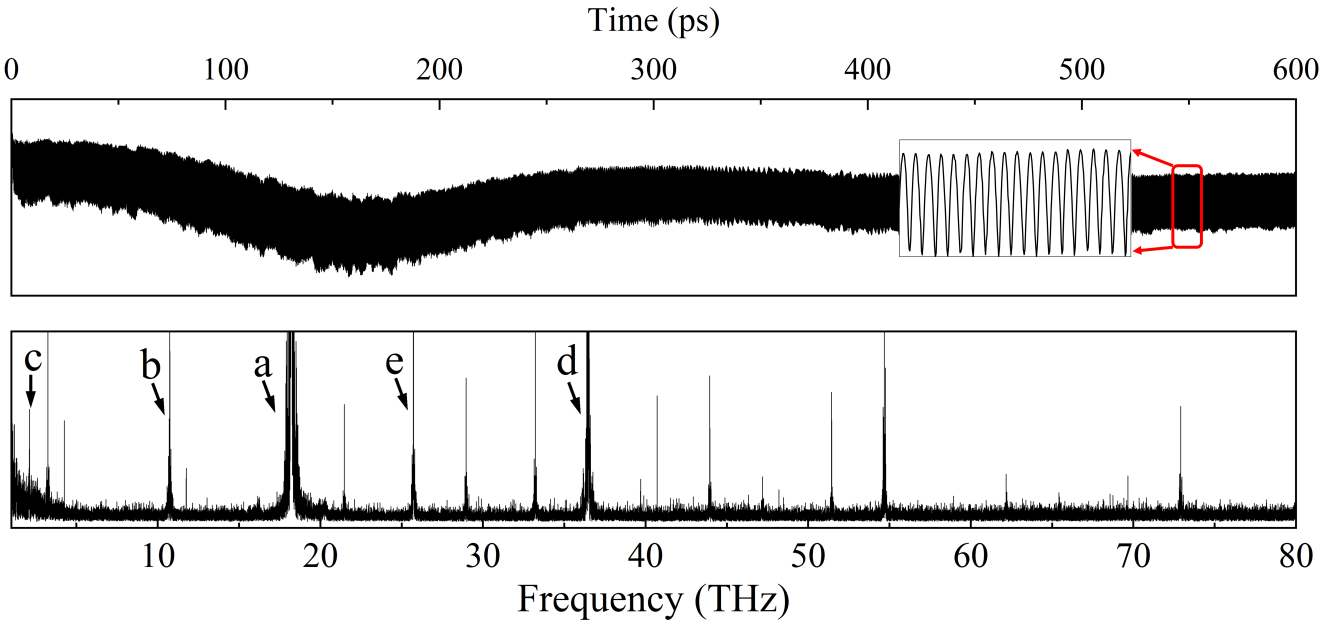

Figure 3.1: Full temporal scan (above) and its respective Fourier transform (below). The inset plot demonstrates the high signal quality and long coherence lifetime. The major features of the Fourier transform are (a) $7S_{1/2} - 5D_{5/2}$ coherence energy difference at 18.225 THz, (b) $8S_{1/2} - 6D_{5/2}$ coherence energy difference at 10.733 THz, (c) $5D_{5/2} - 5P_{3/2}$ and $5P_{3/2} - 5S_{1/2}$ coherence energy differences at 2.109 THz, (d) second harmonic of the 7S-5D coherence, with higher harmonics visible to the right, and (e) one of the many difference frequencies spaced a multiple of 7.49 THz apart from either feature a or b. Scan taken at a rubidium atomic density of 2.6×10^{14} cm^{-3}.

the delay in the response of this coherence could support the idea of excitation through Rb-Rb dimer dissociation, as the dissociation process would not occur at the moment of excitation. The 400 ps is also about twice as long as the average collision time of the vapor, at around 200 ps, lending credibility to the idea of a collisional process being responsible.

3.3 Coherence Control and Fano Simulations

As mentioned previously, the 5S-P-D coherence can be controlled through three primary channels: vapor density, pump-probe crossing angle, and pulse chirp. Changes to two of these settings, vapor density and crossing angle, were observed to produce both a larger magnitude as well as a substantial profile change. An example of this profile is shown in the lower part of Figure 3.2, as well as in Figure 3.6. The notable feature of these profiles is the prominent interference window occurring just past the resonance peak. A series of scans were performed to classify the effect of the previously mentioned variables. The number density was swept from 1×10^{14} cm^{-3} to 4×10^{14} cm^{-3}, and the crossing angle was swept from 0.35 mrad to 1.7 mrad. Pulse chirp, while observed to have some effect on the 5S-P-D profile, is difficult to quantify and control. For the purpose of this thesis, this setting was kept as constant as possible across scans. Some example profiles from these scans are shown in Figure 3.6. Decreasing the number density caused the profile to transition from a sharp resonance peak to a broad, asymmetric profile with defined interference window. Increasing the pump-probe crossing angle causes the same effect, with colinear beams producing narrow profiles, and large angles producing broad, asymmetric profiles.

Due to both the asymmetry of the profile, as well as the apparent interaction between the 5S-P-D and $7S_{1/2} - 5D_{5/2}$ coherences, an effort was made to fit the profiles to the generalized Fano profile described in Chapter 1. These fits were performed only on the main peak in the center of the profile. The large side-bands that appear to both sides of this peak are currently believed to be due to a separate effect, possibly reflections within the vapor cell. For this reason, they are disregarded in the fit. Fits were performed on all profiles captured in the previous experiment. Some examples of these fits are shown in Figure 3.7, overlaid with their respective data sets. Of the

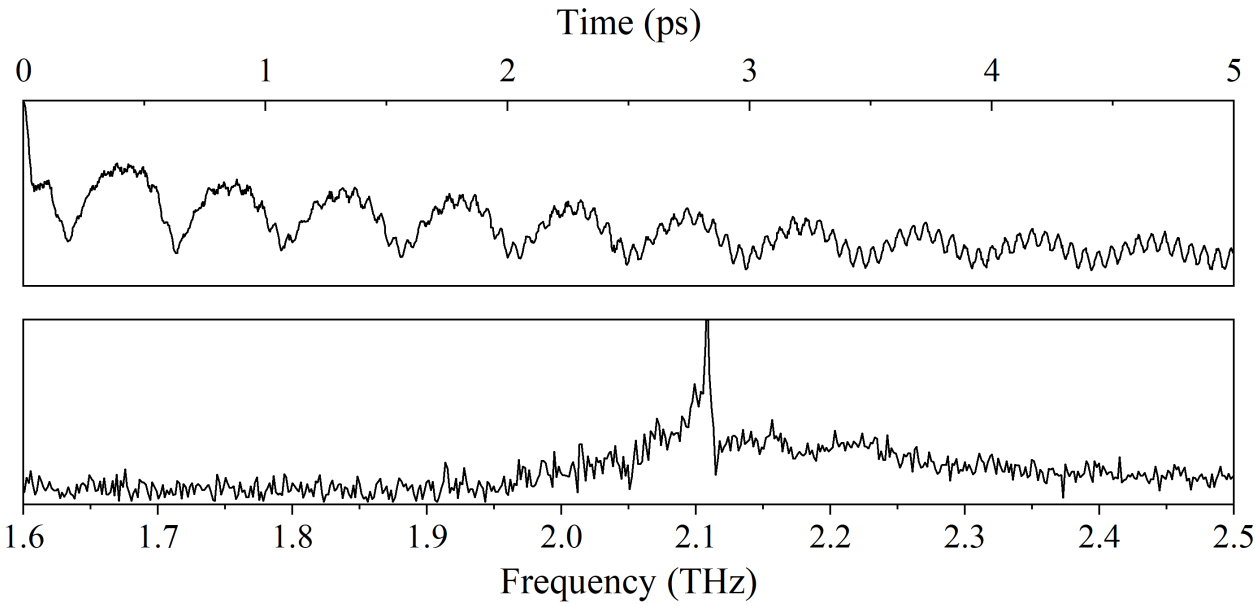

Figure 3.2: Closeup view of 2.1 THz oscillations, with time limited to the first 5 ps following excitation. The 5S-P-D coherence starts off strong before being replaced by the 18 THz $7S_{1/2} - 5D_{5/2}$ coherence. Below is a closeup of the 2.1 THz profile produced via Fourier transform. Scan taken at a rubidium atomic density of 2.6×10^{14} cm^{-3}.

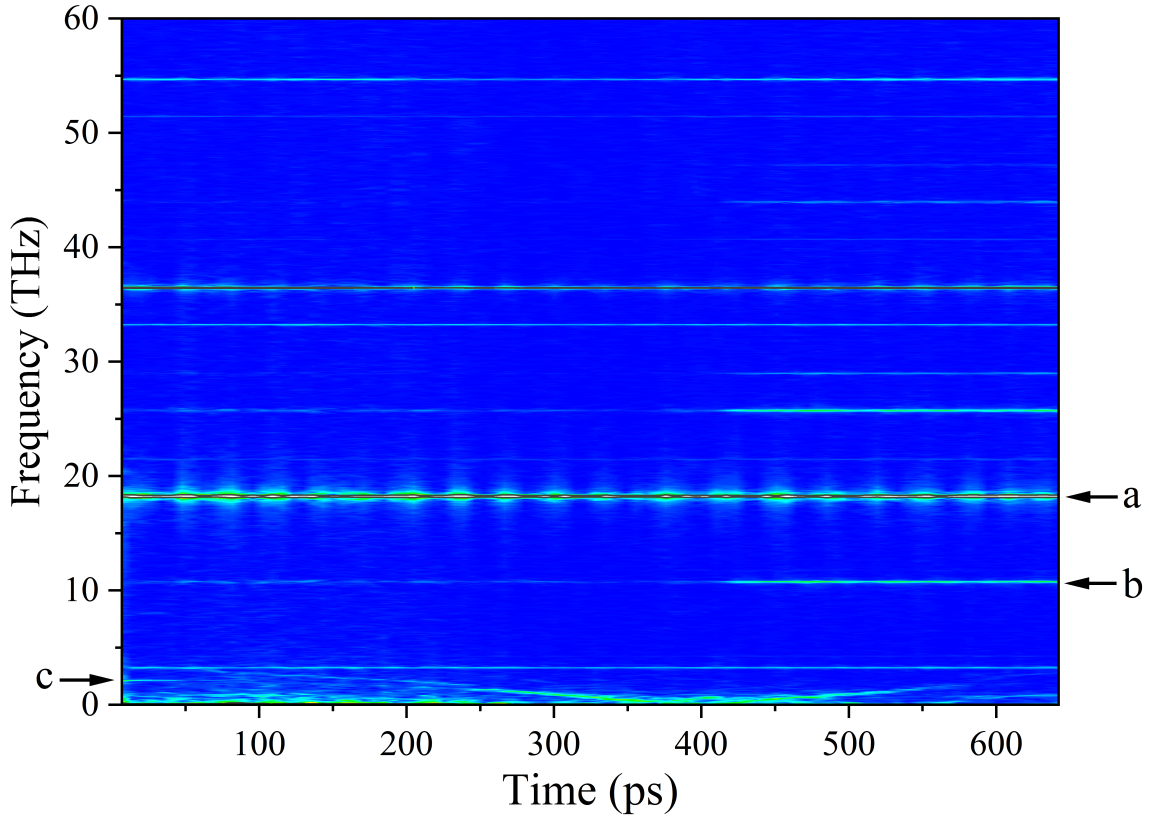

Figure 3.3: Short time Fourier transform of the data presented in Figure 3.1. Features from that figure are labeled the same here: (a) $7S_{1/2} - 5D_{5/2}$ coherence, (b) $8S_{1/2}$ and $6D_{5/2}$ coherence, and (c) 5S-P-D coherence. Performed using a 3 ps rectangular window and 1.5 ps window overlap.

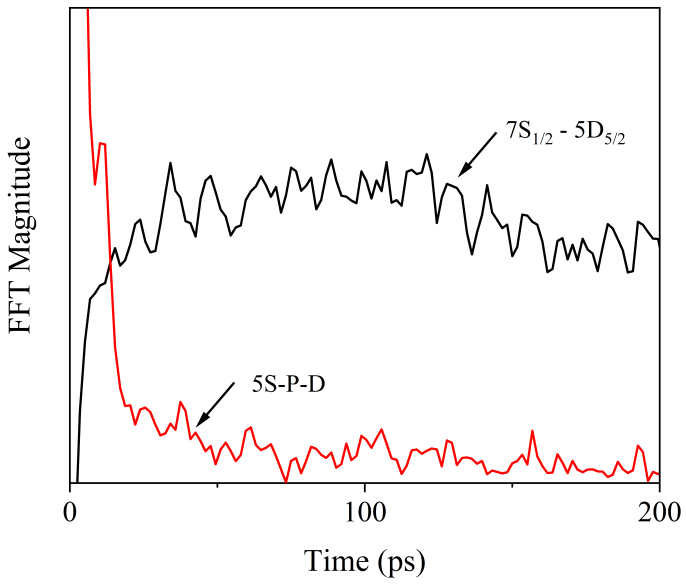

Figure 3.4: Traces of an STFT taken at two different frequencies. The black line represents the temporal evolution of the $7S_{1/2} - 5D_{5/2}$ coherence, while the red line represents the temporal evolution of the 5S-P-D coherence. Simultaneous increase of the $7S_{1/2} - 5D_{5/2}$ coherence and decrease of the 5S-P-D coherence implies a transfer of energy between the two, and possible coupling.

five parameters listed previously, three were identified as having the greatest impact on the quality of the fit. The locations of both the resonance and continuum remained relatively constant, at $E_R = 2.105$ THz and $E_C = 2.114$ THz. The remaining parameters and their response to changing parameters are detailed below:

- Γ_R: The linewidth of the resonance increased with both higher vapor density and lower crossing angle. Varied from $\Gamma_R = 0.015$ to $\Gamma_R = 0.3$ across both parameters.

- Γ_C: The linewidth of the continuum increased with both higher vapor density and lower crossing angle. Varied from $\Gamma_R = 0.05$ to $\Gamma_R = 4$ across both parameters.

- θ: The Fano phase changed abruptly as both vapor density and crossing angle changed, varying from $\frac{\pi}{2}$ to π.

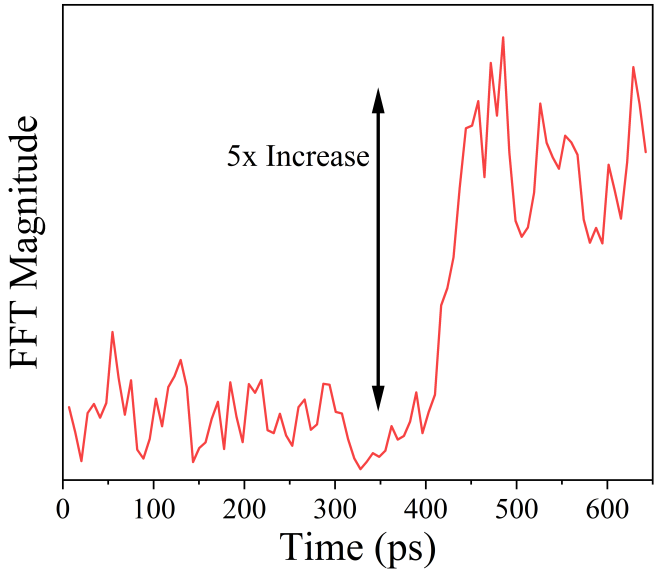

Figure 3.5: Trace of the STFT taken along the $8S_{1/2}$ and $6D_{5/2}$ coherence. There is a sudden increase in the strength of the response by a factor of five occurring around 400 ps. This implies that whatever mechanism excites this coherence takes time, rather than being instant as the others are.

Complete results are presented in the contour plots of Figure 3.8. These show an inverse relationship between number density and pump-probe crossing angle. The smallest values for all three parameters were recorded when number density was at its minimum and crossing angle at its maximum. This seems counterintuitive, as the profiles shown in Figure 3.6 are much broader when the fits seem to call for narrower continuum and resonance widths. However, because the phase is so low, the profiles in this region are dominated by the continuum linewidth, which is an order of magnitude wider than the resonance. This correlates to very weak coupling to the resonance. The narrow resonance linewidth only results in the sharp interference window, and has no effect on the overall shape of the profile in this region. Similarly, largest values were recorded when number density was at its maximum and crossing angle at its minimum. This region is defined by a large phase, correlating to a strong coupling with the resonance and resulting in the dominance of the resonance in the profile. Because of this, the continuum linewidth becomes extraneous in this region, having less impact on the profile as the phase increases. While control over the spectral width of these

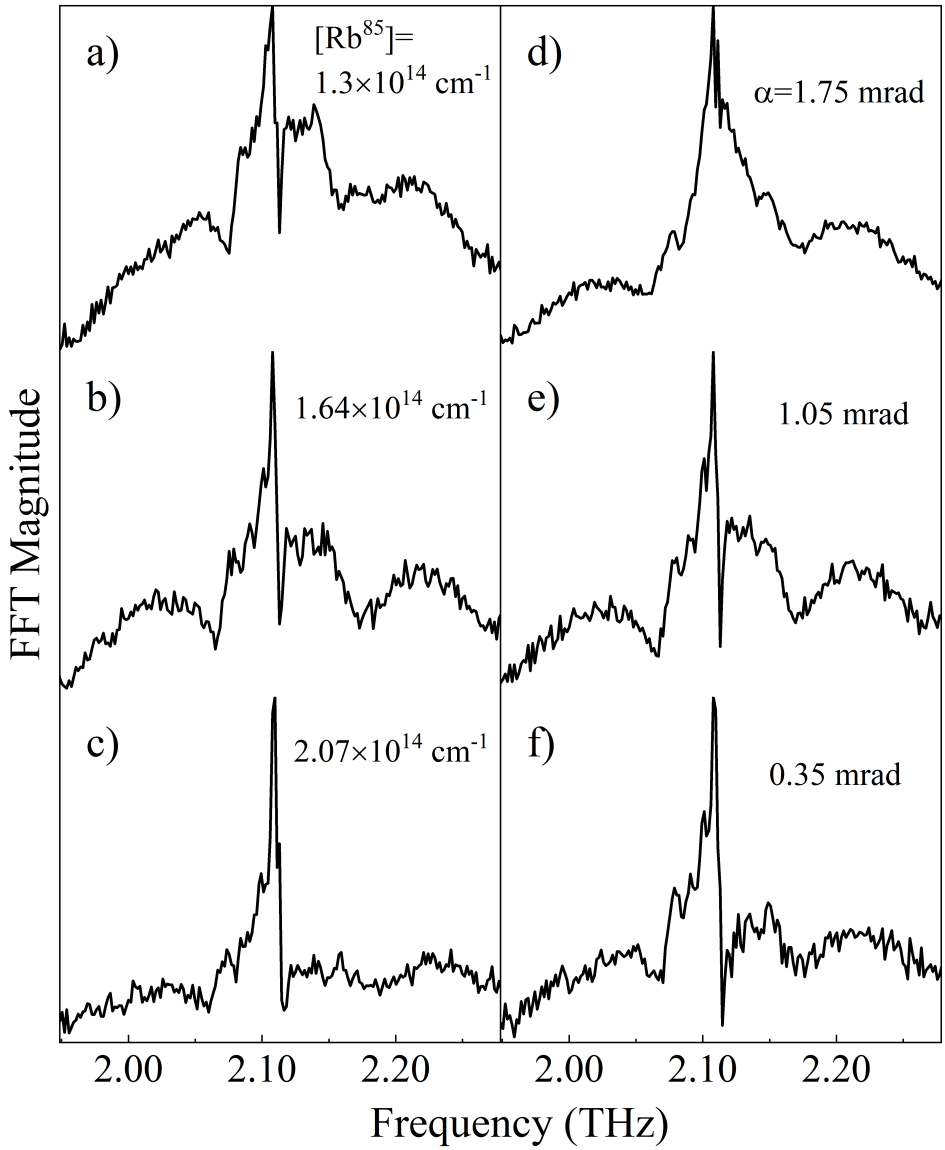

Figure 3.6: Comparisons between profile changes caused by changing number density and crossing angle. Profiles (a)-(c) follow increasing number density, with crossing angle fixed at 0.7 mrad. Profiles (d)-(f) follow decreasing crossing angle, with number density fixed at 1.64×10^{14} cm^{-3}.

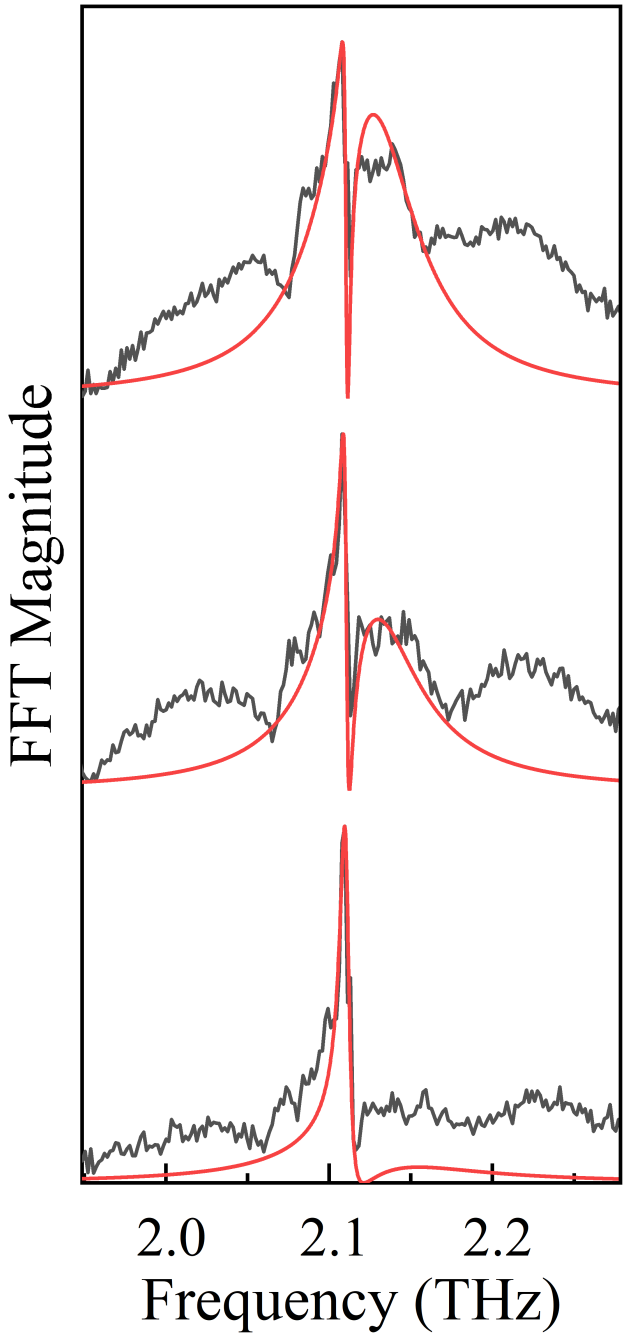

Figure 3.7: Fano profile fit examples. The broad sidebands of the response are ignored during fitting. The profiles shown here are the same as those on the left side of Figure 3.6 (a, b, c).

features is interesting, the ability to transition these resonances from a region of low coupling to high coupling is of utmost importance.

A comparison between the quantitative results of changing crossing angle and number density is shown in Figure 3.9, taken as a cross section of the contour plot in Figure 3.8. As can be seen, regarding the phase, an almost one to one connection between the two variables can be made. Both follow similar trajectories and change the phase to a similar degree. This implies a connection between these two variables, wherein both have the same effect on the sample. This is reinforced by Figure 3.10, which shows the overlap integral of one profile, taken at 2.06×10^{14} cm^{-3} and 1 mrad of crossing angle, and all other profiles. A high overlap value implies the two profiles are very similar, and a band of these high value profiles can be seen stretching toward the upper right. The implication is that it is possible to "undo" the effect of one variable by changing the other. A higher number density can be offset by increasing the crossing angle, and vice versa, to recover what is essentially the same profile. Therefore, the coupling observed within this coherence is controlled by one single parameter, which is able to be adjusted through multiple ways.

Given the non-linear nature of the processes involved as well as the substantial effect crossing angle has on the profile, it is reasonable to assume this underlying parameter is the phase matching condition within the setup. Adjustments to the crossing angle are the easiest way to effect this; however, changes to the number density will change the dispersion of the vapor, allowing indirect control over the phase matching condition. One final clarifying note is that the actual point of proper phase matching is not being changed. Rather, the system is moved closer to or farther away from this ideal condition to produce the profile changes. While it is impossible to know the exact point of complete phase matching, it is possible to quantify the difference in phase matching between profiles.

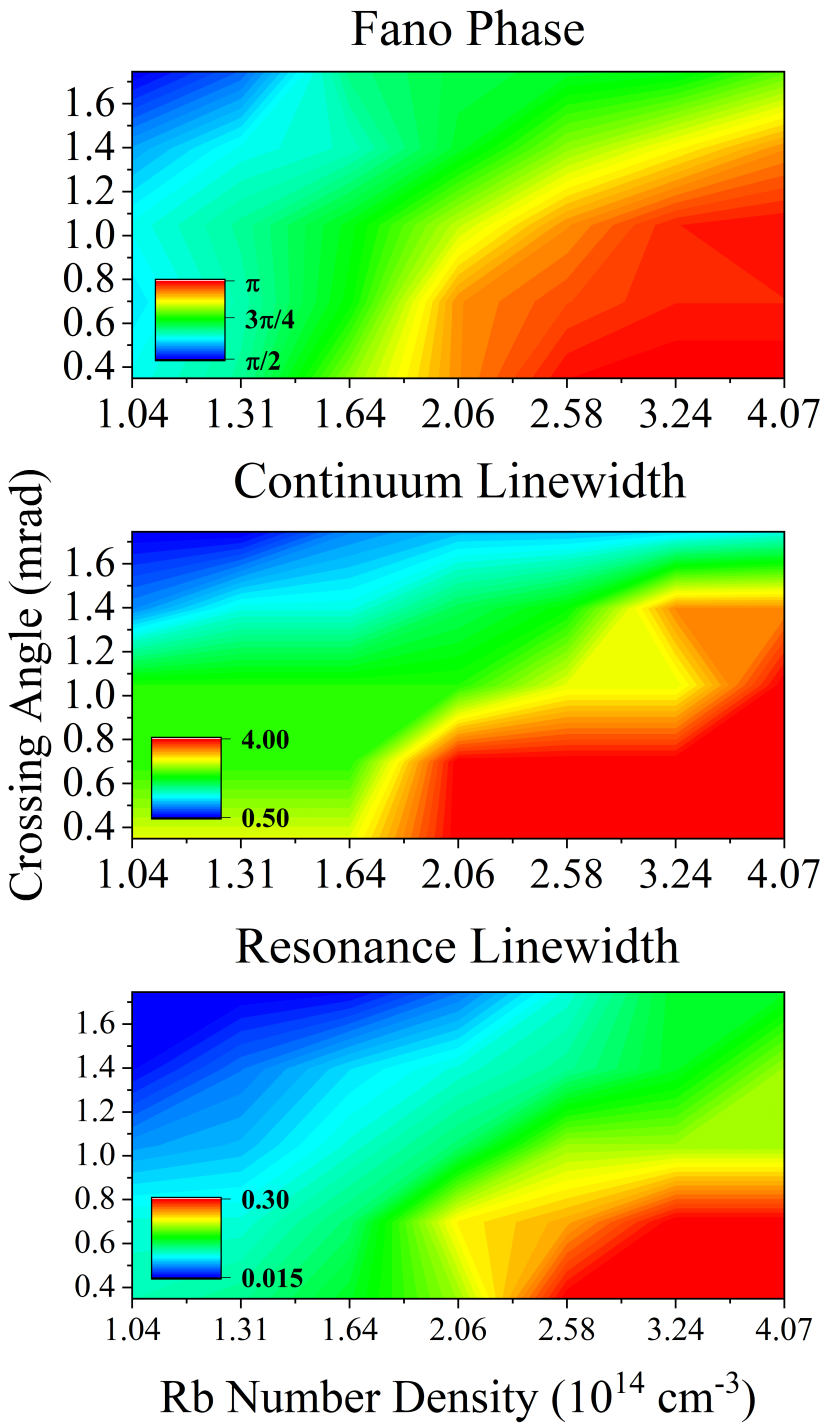

Figure 3.8: Priority fit parameters shown as contour plots. Similar trends are seen across both changing number density and crossing angle.

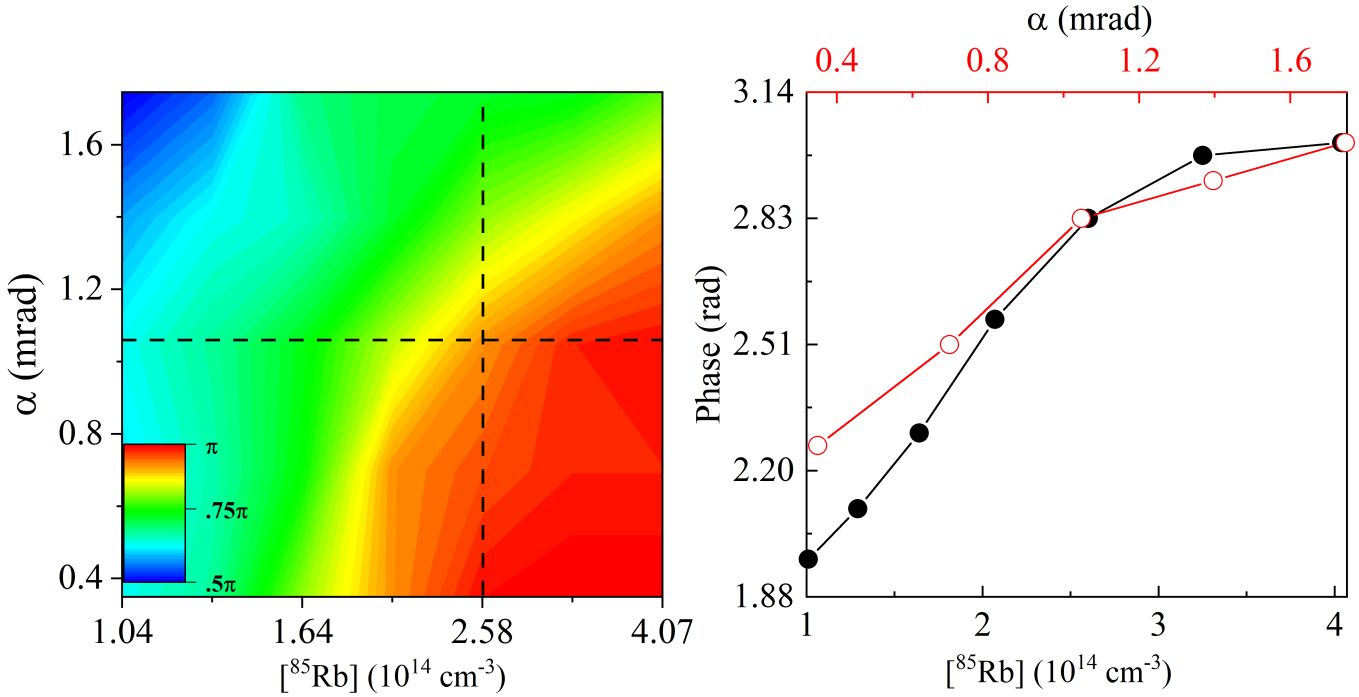

Figure 3.9: Comparison between the numerical effect of changing number density and crossing angle on phase of the profile. Plots to the right correspond to the two dashed black lines on the contour plot to the left. Both variables produce similar changes to the phase of the response, seen as the overlap of the two plots.

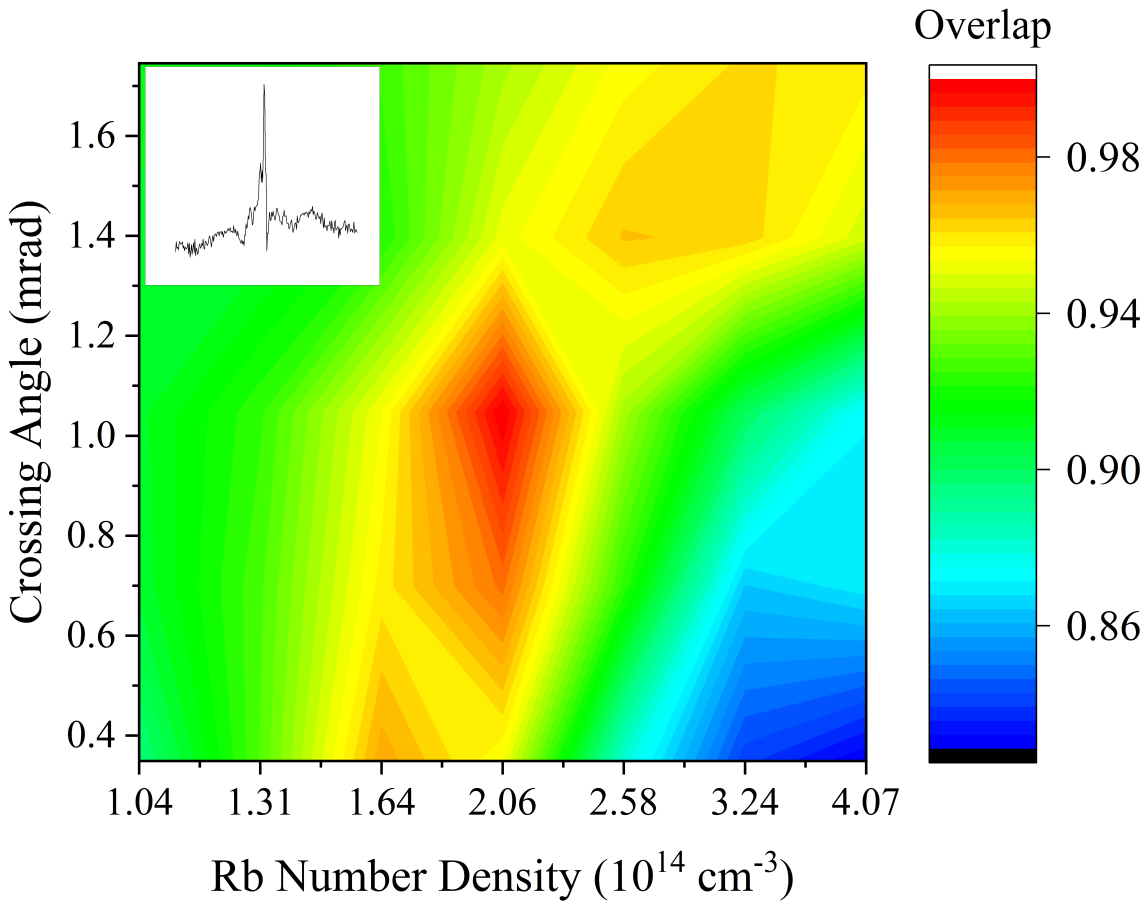

Figure 3.10: Overlap integrals between one profile and all available. The bright red spot is the original profile, also shown in the inset graph, and the yellow band is a range of similar profiles with different number density and crossing angle.

CHAPTER 4

CONCLUSION

This thesis investigated the unique temporal and spectral responses of atomic coherences within Rb through the use of quantum beat spectroscopy. The $5D_{5/2} - 5P_{3/2}$ and $5P_{3/2} - 5S_{1/2}$ pair of coherences proved to be of most interest, as its temporal response was very short lived, and its spectral response produced a unique asymmetric profile. This profile was shown to fit well with a generalized Fano profile, implying coupling between the states. Control over this coupling was also shown to be possible by adjusting the phase matching conditions within the vapor. Further understanding of the processes involved would be of great interest to the world of physics.

Further effort is needed to solidify the claims made in Chapter 3. First and foremost is the need for a defined theory or simulation of the underlying physics. This could be done through the optical Bloch equations or just simple coupled oscillators. This would provide some insight into how the oscillators are truly acting within the atom during excitation. Additional insight could also be gained by looking at other alkali metals. Since their structures are similar, namely the single valence electron and high transition strengths, similar behavior between coherences could be possible. Aside from Rb, quantum beats have already been observed in K, although coupling was not observed [12]. Other alkali metals like Cs should be possible to investigate. Finally, the inclusion of various buffer gasses within the cell could provide some insight into the role of collisions on the excitation process. The cell used in these experiments was entirely evacuated, so collisions were infrequent and only between other Rb atoms. The inclusion of other rare gasses at single Torr pressures should still allow coherences to be established while making collisions more frequent.

REFERENCES

[1] J. P. Home, D. Hanneke, J. D. Jost, J. M. Amini, D. Leibfried, and D. J. Wineland, "Complete methods set for scalable ion trap quantum information processing," *Science*, vol. 325, no. 5945, pp. 1227–1230, 2009.

[2] M. F. Limonov, M. V. Rybin, A. N. Poddubny, and Y. S. Kivshar, "Fano resonances in photonics," *Nature Photonics*, vol. 11, no. 9, pp. 543–554, 2017.

[3] A. Corney and G. W. Series, "Theory of resonance fluorescence excited by modulated or pulsed light," *Proceedings of the Physical Society*, vol. 83, no. 2, pp. 207–212, 1964.

[4] J. N. Dodd, R. D. Kaul, and D. M. Warrington, "The modulation of resonance fluorescence excited by pulsed light," *Proceedings of the Physical Society*, vol. 84, no. 1, pp. 176–178, 1964.

[5] S. Haroche, "Quantum beats and time-resolved fluorescence spectroscopy," in *High-Resolution Laser Spectroscopy*, K. Shimoda, Ed. New York, NY: Springer-Verlag, 1976.

[6] E. Hack and J. R. Huber, "Quantum beat spectroscopy of molecules," *International Reviews in Physical Chemistry*, vol. 10, no. 3, pp. 287–317, 1991.

[7] H. Watanabe, S. Tsuchiya, and S. Koda, "Zeeman quantum beat spectroscopy applied to the A^1A_2–X^1A_1 transition of SO_2," *The Journal of Chemical Physics*, vol. 82, no. 12, pp. 5310–5317, 1985.

[8] T. Walther, H. Bitto, and J. Huber, "High-resolution quantum beat spectroscopy in the electronic ground state of a polyatomic molecule by IR-UV pump-probe method," *Chemical Physics Letters*, vol. 209, no. 5, pp. 455–458, 1993.

[9] W. Goldshlag, "Dynamics of interfering wave packets in rubidium by high resolution quantum beat spectroscopy," Ph.D. dissertation, Univ. of Illinois at Urbana-Champaign, 2017.

[10] K. Shimoda, "Line broadening and narrowing effects," in *High-Resolution Laser Spectroscopy*, K. Shimoda, Ed. New York, NY: Springer-Verlag, 1976.

[11] S. Banerjee and G. Gangopadhyay, "Quantum beat in the pump–probe signal of a molecular system," *Journal of Physics B: Atomic, Molecular and Optical Physics*, vol. 36, no. 14, pp. 2967–2985, June 2003.

[12] H. Tran, P. John, J. Gao, and J. Eden, "Interaction of atomic wave packets with four-wave mixing: Detection of rubidium and potassium wave packets by coherent ultraviolet emission." *Optics Letters*, vol. 23, no. 1, pp. 70–72, 1998.

[13] A. A. Senin, "Study of wavepacket dynamics in rubidium vapor by means of time-frequency analysis," Ph.D. dissertation, Univ. of Illinois at Urbana-Champaign, 2003.

[14] W. Goldshlag, R. Su, S. Park, T. O. Reboli, and J. G. Eden, "Interference between atomic Rb ($5d_{5/2}$–$5p_{3/2}$) and ($5p_{3/2}$–$5s_{1/2}$) coherences: observation of an exceptional point by quantum beating at ∼2.1 THz," *Journal of Physics B: Atomic, Molecular and Optical Physics*, vol. 54, no. 16, p. 165001, 2021.

[15] A. Kramida, Yu. Ralchenko, J. Reader, and NIST ASD Team, NIST Atomic Spectra Database (ver. 5.9), [Online]. Available:`https://physics.nist.gov/asd` [2022, April 2]. National Institute of Standards and Technology, Gaithersburg, MD, 2021.

[16] U. Fano, "Effects of configuration interaction on intensities and phase shifts," *Physical Review*, vol. 124, no. 6, pp. 1866–1878, 1961.

[17] P. Durand, I. Paidarová, and F. X. Gadéa, "Theory of Fano profiles," *Journal of Physics B: Atomic, Molecular and Optical Physics*, vol. 34, no. 10, pp. 1953–1966, 2001.

[18] Y. S. Joe, A. M. Satanin, and C. S. Kim, "Classical analogy of Fano resonances," *Physica Scripta*, vol. 74, no. 2, pp. 259–266, 2006.

[19] R. Su, "Probing weakly bound long-range Rydberg molecules by quantum beating experiments in rubidium vapor," Ph.D. dissertation, Univ. of Illinois at Urbana-Champaign, 2020.